Primljen / Received: 10.9.2024.
Ispravljen / Corrected: 22.9.2025.
Prihvaćen / Accepted: 29.9.2025..
Dostupno online / Available online: 10.1.2026.

Analysis of force characteristics of "pile-wall" structure based on elastic foundation beam method

Authors:

[1]Bo Zhang
zhangbo6@sdepci.com

[1]Jiabin Xu
xujiabin@sdepci.com

[1]Xiuqin Shi
shixiuqin@sdepci.com

[1]Na Chen
chenna@sdepci.com

[1]Yucai Dong
dongyucai@sdepci.com

[2,3,4]Prof. Huanwei Wei
13181718169@163.com

[2,3,4]Pengyue Wang, MSc. CE
wpy1029392119@126.com
Corresponding author

[1] Shandong Electric Power Engineering Consulting Institute Corp. Ltd, China
[2] Shandong Jianzhu University, China
[3] Key Laboratory of Building Structural Retrofittingand Underground Space Engineering Ministry of Education
[4] Subway Protection Research Institute

Research Paper

Bo Zhang, Jiabin Xu, Xiuqin Shi, Na Chen, Yucai Dong, Huanwei Wei, Pengyue Wang

Analysis of force characteristics of "pile-wall" structure based on elastic foundation beam method

A dual-purpose wall structural system considers temporary perimeter piles as part of the underground structure in normal stage; however, there is a lack of effective theoretical formulas to predict node reinforcement forces, pile wall internal force patterns, and load-sharing characteristics. To analyse the force characteristics of the dual-purpose wall structure, we established a simplified model to derive the internal force equations of the pile wall and nodes with and without connection nodes. Subsequently, we analysed the pile–wall internal force of the dual-purpose wall structural system and the internal force of the pile wall with and without connection nodes using finite element software. The results show that analytical solutions of the pile wall agree well with the numerical simulation results, and that the derived formulas for the pile-wall internal forces are reliable. These results deepen our understanding of the force characteristics of dual-purpose wall structures, which can be used as a theoretical basis for the promotion of dual-purpose wall structures in engineering design.

Key words:
dual-purpose wall, computational model, theoretical deduction, numerical simulation, internal force analysis

Prethodno priopćenje

Bo Zhang, Jiabin Xu, Xiuqin Shi, Na Chen, Yucai Dong, Huanwei Wei, Pengyue Wang

Analiza karakteristika sila kod konstrukcije pilot – zid primjenom metode grede na elastičnoj podlozi

U konstruktivnome sustavu zidova s dvostrukom namjenom privremeni obodni piloti koriste se i kao dio podzemne konstrukcije tijekom normalne faze upotrebe. Međutim, postoji nedostatak učinkovitih teorijskih formulacija za predviđanje sila u točkastim ojačanjima, raspodjele unutarnjih sila u konstrukciji pilot – zid i karakteristika raspodjele opterećenja. Kako bi se analizirale značajke sila u konstrukciji zida s dvostrukom namjenom, razvijen je pojednostavljeni model za izvođenje izraza unutarnjih sila u sustavu pilot – zid i u čvorovima, sa spojnim čvorovima i bez njih. Također, analizirane su unutarnje sile u sustavu pilot – zid s dvostrukom namjenom te su uspoređene unutarnje sile sustava u slučajevima sa spojnim čvorovima i bez njih primjenom računalnog programa temeljenog na metodi konačnih elemenata. Rezultati pokazuju da se analitička rješenja sustava pilot – zid dobro podudaraju s rezultatima numeričke simulacije te da su izvedeni izrazi za unutarnje sile sustava pouzdani. Ti rezultati produbljuju razumijevanje karakteristika sila konstrukcija s dvostrukom namjenom i mogu poslužiti kao teorijska osnova za njihovu primjenu u projektiranju.

Ključne riječi:
zid s dvostrukom namjenom, računalni model, teorijska dedukcija, numerička simulacija, analiza unutarnjih sila

1. Introduction

Current excavation support systems in soft-soil areas often rely on numerous cast-in-place concrete piles, inner supports, and anchors as temporary structures. These piles are usually left in ground after the construction of the basement structure is completed, resulting in substantial solid waste in the stratum around the excavation site. This practice causes several issues, including high energy consumption, resource wastages, and environmental pollution. Perimeter piles are designed as bending members, and their stiffness is generally high; therefore, they can continue to function as members even after the excavation is complete. If a basement wall and the retaining piles of the excavation are combined, such that the retaining piles serve as part of the basement wall during the permanent use phase, i.e., the "pile-wall" technology [1], the thickness of the basement wall can be reduced. This approach enables the excavation support structure to achieve energy-savings and promotes sustainable development. The technology has broad application prospects and significant social and economic benefits, prompting extensive research by both domestic and international scholars.

Wang et al. [2] examined the waterproofing and force transmission behaviour of the "pile-wall" technology and performed strength and durability calculations under multiple working conditions such as the excavation stage, normal use stage, and seismic conditions. Nie et al. [3] studied the elastic and elasto-plastic bending characteristics of axially variable stiffness beams under minimal deformation conditions and derived analytical solutions for their elastic and elasto-plastic deformations when the height of the cross-section and the modulus of elasticity of the material was varied according to a special function along the length of the beam. Hu et al. [4] studied an excavation project in Shanghai Hongqiao Business District and conducted stress measurements on the "pile-wall" structural system from the excavation base to the construction of a superstructure, deepening the understanding of the stress characteristics of the "pile-wall" structural system. Wang et al. [5] examined a deep excavation project for a rainwater storage pond in Hefei City, focusing on the structural design and construction methods of the "pile-wall" technology. They detailed the entire construction process of construction stage and analysed the monitoring data to demonstrate the applicability of the technology in practice. Zhong et al. [6] demonstrated the application of "pile-wall" technology in real-world engineering through a case study of Lot 8 of Hongqiao Business District and proposed the overall idea of "pile-wall" design and construction measures.

In practical engineering, excavation projects are not limited to clayey strata; sandy, gravelly, and mixed soils (e.g. silty sand) are widely distributed in coastal, river valley, and mountainous areas [7]. These granular soils exhibit distinct mechanical properties compared to clayey soil (e.g., low cohesion, high internal friction angle, and strong permeability). Nevertheless, the core theoretical framework of the "pile-wall" structure employed in this study, including the Euler–Bernoulli beam assumption, Rankine earth pressure theory, and elastic foundation beam method, is inherently adaptable to multiple soil types. In particular, the Rankine earth pressure theory, which forms the basis of external pressure calculation in this paper, can be directly applied to sandy/gravelly soil by adjusting key parameters, such as setting cohesion (c) as 0 for cohesionless soil [8].

At present, the pile-wall structure can be divided into clingy and separation "pile-wall" structures based on their structural forms. In a clingy "pile-wall" structure, the retaining piles are connected with the basement wall through connection nodes such as rebars, integrating both elements into a single composite system. This configuration enhances the cross-section bending stiffness, and it is usually used in deep excavations [9]. In contrast, a separate "pile-wall" structure incorporates horizontal force-transmitting members in the basement slab to transfer the soil pressure on the retaining piles to the basement slab, thereby reducing the load acting on the basement wall.

The application of "pile-wall" technology in excavation projects remains relatively remains relatively limited compared with other supporting structures. Existing cases, such as the Tianjin Jinmen Excavation Project and Shanghai Chest Hospital Lung Cancer Clinical Medical Centre Ward Building Project, have primarily adopted the technology passively, by stacking retaining piles and basement walls within constrained structural spaces. This study focuses on the "pile-wall" structure by developing a simplified calculation model of the "pile-wall" structure and performing numerical simulation using the Plaxis 3D finite element simulation software to verify the correctness and accuracy of the simplified model.

2. Derivation of formulae in pile-wall

2.1. Equation for internal force with connection nodes

Based on the structural characteristics and force-bearing conditions of the retaining piles and basement wall, the following simplifications were applied for developing the model (Fig. 1):

- Given a sufficient number of retaining piles arranged along the length direction and the adequate extension length of the basement wall, a single retaining pile and segment of the basement wall (with the same vertical length as the retaining pile) were selected as research objects. To minimize boundary effects, the vertical section along the Z-direction at the mid-span of the structure was analysed.
- The retaining pile and basement wall were treated as two vertical Euler–Bernoulli (EB) beams. As both members are made of reinforced concrete, they share the same elastic modulus; however, their cross-sectional heights differ.
- Because the widths of the two beams did not affect the calculation results of the structural internal forces, their widths were assumed to be equal for simplicity (both are denoted by b).

Regarding the boundary constraints, the top and bottom slabs of the basement wall exhibit high stiffness in actual excavation projects. As these slabs are directly connected to the basement wall, their lateral deformation under load is minimal. The connection locations are shown as points A and B in Fig. 1. Thus, the constraint at points A and B was modelled as a hinged support. The bottom of the retaining pile interacts with the surrounding soil, which provides elastic resistance; hence, point C was modelled as a spring-bearing constraint.

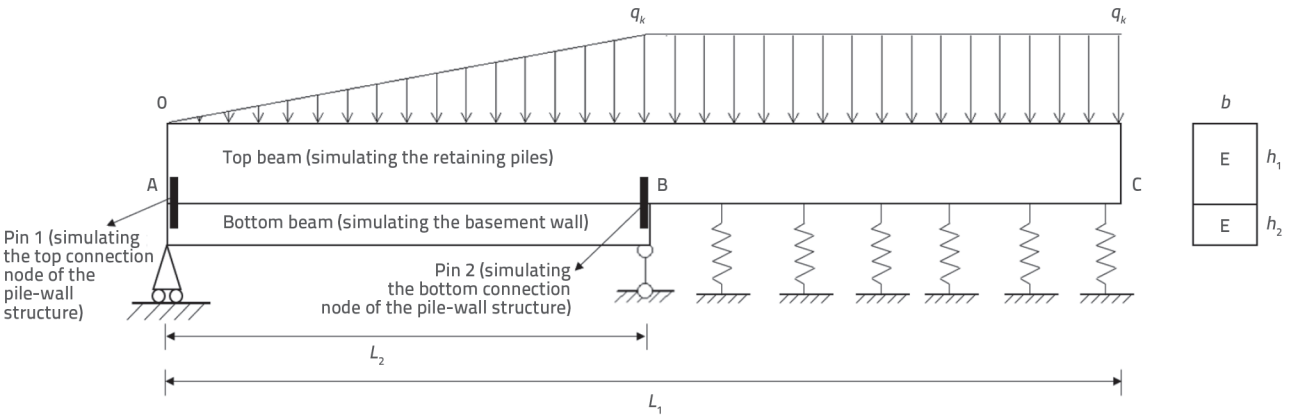

Figure 1. Simplified model diagram for Z-direction structural calculations

The top beam, which simulates the retaining pile, and the bottom beam, which simulates the basement wall, were stacked together, and the connection nodes between the retaining pile and basement wall were simulated using the pins at points A and B. Pin 1 at point A represents the connection node at the top of the pile wall structure, and pin 2 at point B represents the connection node at the bottom of the pile wall structure. The contact surfaces of the two beams is assumed to be non-adhesive.

2.1.1. Calculation of external pressure

The earth pressure acting on the retaining piles was calculated according to the Rankine active earth pressure theory. The earth pressure below the excavation surface was assumed to follow a rectangular distribution, as shown in Fig. 1. The magnitude of the pressure was determined based on the Rankine formulation for active earth pressure in clay and silt soils [10].

$$K_a = \tan^2\left(45^\circ - \frac{\varphi}{2}\right) \tag{1}$$

$$z_0 = \frac{2c}{\gamma \cdot \sqrt{K_a}} \tag{2}$$

$$E_{a1} = (H - z_0) \cdot \left(\gamma H K_a - 2 \cdot \frac{\sqrt{K_a}}{2}\right) \tag{3}$$

$$E_{a2} = \frac{1}{2} \cdot \gamma H^2 K_a - 2cH \cdot \sqrt{K_a} + \frac{2c^2}{\gamma} \tag{4}$$

where

- φ - the angle of internal friction of the soil
- K_a - the Rankine active earth pressure coefficient
- c - the cohesion of the soil
- γ - the gravity of the soil
- z_0 - the critical depth (the depth of the calculation point from the surface of the ground)
- E_{a1} - he active earth pressure of the cohesive soil
- E_{a2} - the active earth pressure of the silty soil.

Eqs. (1) to (4) can be used to determine the specific value of the external earth pressure (q_k) acting on the top beam to simulate the external earth pressure of the retaining pile, as shown in Fig. 1.

2.1.2. Hinged support forces in the simplified structure

A simplified pile wall model is shown in Fig. 1. The geometric and material parameters of the model are defined as follows:

- The top beam, which simulates the retaining pile, has a cross-sectional height of h_1 and total length of L_1.
- The bottom beam, which simulates the basement wall, has a cross-sectional height of h_2 and total length of L_2.
- The overlapping length of the two beams is L_2.
- Both the top and bottom beams are made of reinforced concrete with a consistent elastic modulus, denoted as E.

In this simplified model, segment AB exhibits the mechanical behaviour of an overlapping beam. To analyse its structural force characteristics, the bending stiffness formulation bimodal material beams was introduced [9]. Based on this formula, segment AB can be treated as a beam segment with an equivalent bending stiffness denoted as EI_3, which is expressed as follows:

$$EI_3 = \frac{b}{3}\left[E \cdot \left(\frac{h_1 + h_2}{2}\right)^3 \cdot 2\right] = \frac{Eb(h_1 + h_2)^3}{12} \tag{5}$$

where b denotes the width of the top and bottom beams.

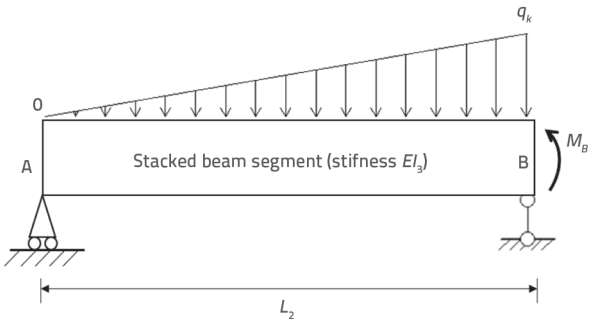

Figure 2. Simplified modelling of stacked beam segments

The segment BC was still a segment with a bending rigidity of EI_1. Because the hinged supports were located in the overlapping segment of the basement wall and retaining pile, from the excavation base to the surface of the earth, the internal forces of the stacked segment were analysed individually. Because the beam of segment BC was embedded in the soil below the excavation base, Point B was simplified as a fixed bearing. A simplified model is shown in Fig. 2.

The two hinged supports at points A and B are assumed to provide only the support reaction force. Therefore, the deflection of the simplified model (Fig. 2) at point A is caused by the soil pressure q_k and support reaction forces F_A and F_B. Assuming that the deflections at point B under the independent actions of the external load q_k and the additional unknown bending moment M_b generated by the fixed support are denoted as θ_{Bq} and θ_{BM} respectively (as shown in Fig. 3), the overall structural response can be determined. Based on the principles of superposition, compatibility, and geometric consistency, the following geometric relationship can be established:

$$\theta_{Bq} + \theta_{BM} = 0 \tag{6}$$

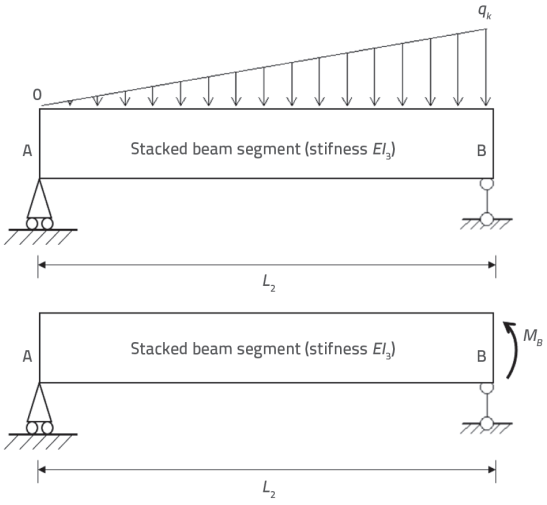

Figure 3. Superposition of forces in the stacked beam

The physical relationship between force and deflection can be obtained from the mechanics of the materials as follows:

$$\theta_{Bq} = \frac{q_k L_2^3}{45EI_3} \tag{7}$$

$$\theta_{BM} = -\frac{M_B L_2}{3EI_3} \tag{8}$$

Substituting Eqs. (7) and (8) into Eq. (6), bending moment M_B of fixed support B can be solved as follows:

$$M_B = \frac{q_k L_2^2}{15} \tag{9}$$

From this, the static equilibrium equations can be obtained:

$$F_A L_2 + \frac{q_k L_2^2}{15} + \frac{L_2}{3} \cdot \frac{q_k L_2}{2} = 0 \tag{10}$$

Therefore, we can conclude that the reaction force F_A of the hinged support at A:

$$F_A = \frac{7q_k L_2}{30} \tag{11}$$

2.1.3. Internal force of the structure solution

The bending stress and shear force of the structure are illustrated in Fig. 4. To determine the changing pattern between the different positions in the cross section of the stacked beam segment AB (denoted by y) and the linear strain of y, the linear strain [11] can be solved by assuming a the plane cross section.

$$\varepsilon = \frac{y}{\rho} \tag{12}$$

Here, y denotes the distance from any calculation point in the cross-section of the stacked beam to the neutral layer of the stacked beam, and ρ denotes the radius of curvature of the neutral layer of the stacked beam.

Without considering the mutual extrusion in the longitudinal direction of the stacked beams, it is assumed that all calculation points of the stacked beam cross-section experience an unidirectional force under ideal conditions. According to Hooke"s law, the positive stress in the cross-section is given by

$$\sigma = E\varepsilon \tag{13}$$

Zamjenom izraza (12) u (13) dobiva se izraz (14):By substituting Eq. (12) into Eq. (13), we obtain Eq. (14) as follows:

$$\sigma = \frac{Ey}{\rho} \tag{14}$$

In the simplified model shown in Fig. 4, the total axial force on the cross-section AB in the stacked beam was 0.

$$\sum F_N = \int_{A_1} \sigma_1 dA + \int_{A_2} \sigma_2 dA = 0 \tag{15}$$

where:

σ_1 - the stress in the cross-section of the top beam within the stacked AB segment

σ_2 - the stress in the cross-section of the bottom beam within the stacked segment AB

A_1 & A_2 - the cross-sectional area of the top beam within the stacked segment AB, and A_2 is the cross-sectional area of the bottom beam within the stacked segment AB

By substituting Eq. (14) into Eq. (15) and defining y_0 as the distance from the neutral axis of the cross-section of the stacked beam to the laminated surface between the top and bottom beams the stacked section of AB, Eq. (16) can be derived as follows:

$$-\int_0^{-y_0} \frac{Ey}{\rho} dy - \int_{-x}^{-(x+h_2)} \frac{Ey}{\rho} dy + \int_0^{h_1-x} \frac{Ey}{\rho} dy = 0 \tag{16}$$

Furthermore, y_0 can be derived from Eq. (16) as follows:

$$y_0 = \frac{h_1 - h_2}{2} \tag{17}$$

Considering the left part of the structure shown in Fig. 4 for force analysis, the bending moment is evaluated at the position of the laminated surface between the top and bottom beams on the cross-section of the stacked beams. Let M_1 and M_2 denote the bending moments in the cross-section of the top and bottom beams, respectively, and x is the distance from any position of the stacked beams to point A, which corresponds to the ground surface in practical engineering (Fig. 4). Thus, based on the principles of mechanics of materials, the equilibrium condition of the cross-section of the structure in Fig. 4 can be expressed as follows:

$$M_1 + M_2 + \int_{-h_2-y_0}^{h_1-y_0} \frac{Eb \cdot y}{\rho} \cdot y dy + F_A x - \frac{q_k x^3}{6L_2} = 0 \tag{18}$$

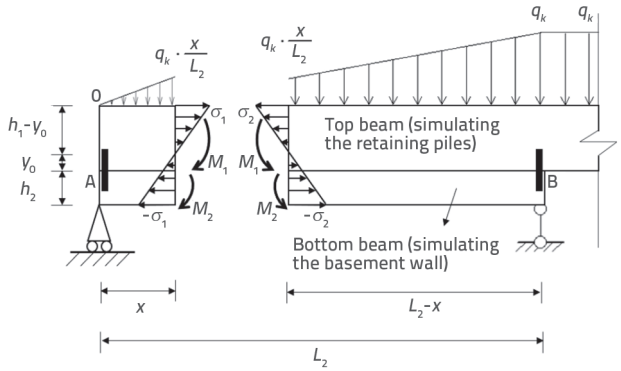

Figure 4. Force diagram of a stacked beam with connected nodes

Based on a previous study [12], the relationship between the bending moment of the laminated beam and the radius of curvature in the cross-section shown in Fig. 4 can be expressed as follows:

$$\frac{1}{\rho} = \frac{M_1 + M_2}{EI_3} \tag{19}$$

Because the top and bottom of the model structure shown in Fig. 4 have connection nodes, the middle layer of the stacked beam remains unchanged when the stacked beam is bent under force. Eq. (20) can be established as

$$\frac{M_1}{EI_1} = \frac{M_2}{EI_2} \tag{20}$$

Thus, we obtain three static equilibrium equations (Eqs. (18–20)). By combining Eqs. (18–20), we obtain

$$M_1 = \frac{h_1^3}{2(h_1^3 + h_2^3)} \cdot \left(\frac{q_k x^3}{6L_2} - \frac{7q_k L_2}{30} \cdot x \right) \tag{21}$$

$$M_2 = \frac{h_2^3}{2(h_1^3 + h_2^3)} \cdot \left(\frac{q_k x^3}{6L_2} - \frac{7q_k L_2}{30} \cdot x \right) \tag{22}$$

where F_A is a constant that can be solved using Eq. (11).
Therefore, the bending moment distribution in segment AB of the perimeter pile, which represents the perimeter pile from the surface to the excavation floor with depth x (Fig. 4), is given by Eq. (21). Similarly, the variation in the bending moment in segment AB of the basement wall, from the surface to the excavation floor with depth x (Fig. 4), is given by Eq. (22).
Because the connection nodes at the top and bottom of the stacked beam combine the retaining pile with the basement wall, pin 1 (Fig. 4 on the left side) and pin 2 (Fig. 4 on the right side) experience equal shear forces, which are given by

$$Q_p = \int_0^{-y_0} \frac{Eb}{\rho} y dy = \frac{3(h_1 - h_2)^2}{4(h_1 + h_2)^3} \cdot \left(\frac{q_k x^3}{6L_2} - \frac{7q_k L_2 x}{30} \right) \tag{23}$$

where b is the width of stacked beam including the top and bottom beams, ρ is the radius of curvature of the neutral layer of the stacked beam, and y_0 is the distance from the neutral layer of the cross-section of AB segment in the stacked beam to the laminated surface of the two beams. y_0 is a constant, and its value is given by Eq. (17).
The bending moment of the connection nodes M_p between the top and bottom beams, which simulate the retaining pile and basement wall, respectively, is obtained by superimposing the section moments of the top and bottom beams (M_1 and M_2, respectively) at depth x, corresponding to excavation L_2.

$$M_p = \frac{1}{2} \cdot \left(\frac{q_k L_2^3}{6L_2} - \frac{7q_k L_2^2}{30} \right) \tag{24}$$

2.2. Equation for internal force without connection nodes

The left part of the structure is shown in Fig. 5 for force analysis. The bending moment can be taken as the position of the laminated surface between the top and bottom beams; M_3 and M_4 are the cross-sectional bending moments of the top and bottom beams, respectively; and x is the distance from any position of the stacked beam to point A at the ground surface (Fig. 4). Therefore, based on the theory of static equilibrium, the cross-section equilibrium condition of the structure shown in Fig. 4 is

$$\int_{-0.5h_1}^{0.5h_1} \frac{Eb \cdot y}{\rho_3} \cdot (y + \frac{h_1}{2}) dy + \int_{-0.5h_2}^{0.5h_2} \frac{Eb \cdot y}{\rho_4} \cdot (y + \frac{h_2}{2}) dy + \\ + F_A x - \frac{q_k x^3}{6L_2} + M_3 + M_4 = 0 \tag{25}$$

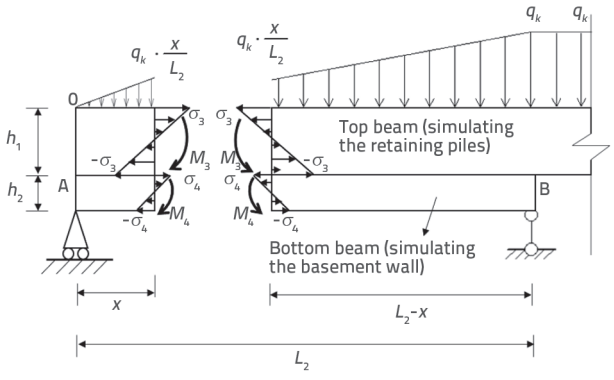

Figure 5. Force diagram of the stacked beam without connected nodes

Based on a previous study [11], the relationship between the bending moment and the radius of curvature in the cross-section of the top and bottom beams shown in Fig. 5 is as follows:

$$\frac{1}{\rho_3}=\frac{M_3}{EI_1} \tag{26}$$

$$\frac{1}{\rho_4}=\frac{M_4}{EI_2} \tag{27}$$

Since the model structure shown in Fig. 5 has no fixed constraints at the connection nodes on the top and bottom beams, and the two beams are only in contact with each other, the curvature of the laminated surface of the two beams is equal. In other words, the longitudinal deformations of the two beams are equal, resulting in the following relationship:

$$N_3=\int_{-y_0}^{h_1-y_0}\frac{Eb}{\rho}\cdot ydy=\frac{Eb}{2\rho}h_1h_2 \tag{28}$$

$$N_4=\int_{-(y_0+h_2)}^{-y_0}\frac{Eb}{\rho}\cdot ydy=-\frac{Eb}{2\rho}h_1h_2 \tag{29}$$

$$\int_0^{L_2}\left(\frac{N_3}{EA_1}-\frac{M_3h_1}{2EI_1}\right)dx=\int_0^{L_2}\left(\frac{N_4}{EA_2}+\frac{M_4h_2}{2EI_2}\right)dx \tag{30}$$

Here, N_3 and N_4 are the total axial forces of the top and bottom beams, respectively, of segment AB of the stacked beam. Combining Eq. (25) to (30), we get

$$M_3=\frac{h_1^3(h_1+2h_2)}{2(h_1+h_2)^2(h_1^2-h_2^2)}\cdot\left(\frac{q_kx^3}{6L_2}-\frac{7q_kL_2}{30}\cdot x\right) \tag{31}$$

$$M_4=-\frac{h_2^3(2h_1+h_2)}{2(h_1+h_2)^2(h_1^2-h_2^2)}\cdot\left(\frac{q_kx^3}{6L_2}-\frac{7q_kL_2}{30}\cdot x\right) \tag{32}$$

where F_A is a constant, and its value is shown in Eq. (11).

3. Finite element comparison

3.1. Engineering background

The project is in Leopard Creek Greenland Park, at the intersection of Shendun 3rd Road and Guanggu 4th Road in Guanggu Centre City, Wuhan City, Hubei Province. The site lies within the geomorphological unit of the Yangtze River III terraced stripped Longgang zone and consists a slopped land formed by multi-phase landfill, with the higher elevation in the northeast and lower elevation in the southwest. Site investigations indicate that the soil in the proposed site ranges from soil to medium hard. Due to the relatively deeper excavation and the narrow space around the basement perimeter from the red line of the site closer, a combination of perimeter piles and internal support joint blocking was used for excavation retaining. The specific tightly adhering to the type "pile-wall" excavation engineering structure section shown in Fig. 6. To address the waterproofing requirement of the "pile-wall" structure in this project, two key measures are adopted based on the site"s perched groundwater distribution (confined to the southwestern low-lying filled area) and stratum characteristics (silty clay, clay with low permeability):

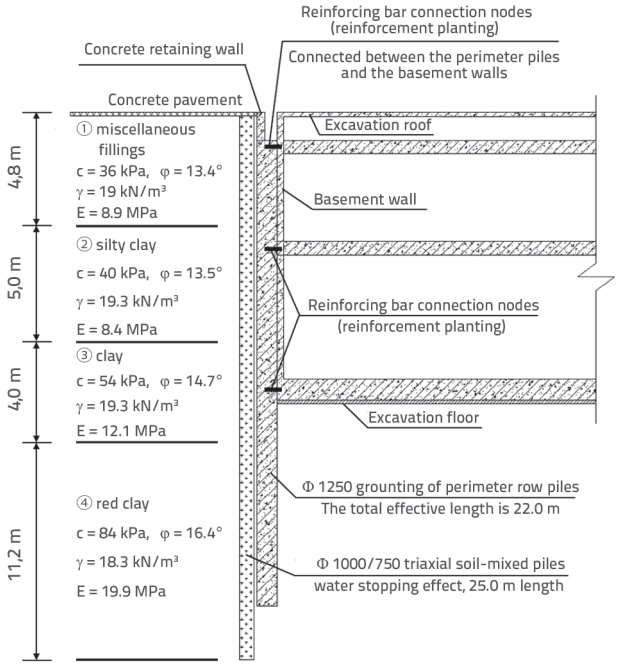

Figure 6. Cross-section of clingy "pile-wall" structure

Waterproofing at pile-wall connection nodes

The rebar connection nodes (reinforcement planting shown in Fig. 6) between the perimeter piles and basement walls were treated with polymer cement waterproof mortar, and a 2-mm thick polyurethane waterproof coating was applied to the joint surface, which prevented groundwater seepage along the rebar gaps and ensured the integrity of the waterproof layer.

Waterproofing between retaining piles:

As shown in Fig. 6, Φ1000/750 triaxial soil-mixed piles (length: 25.0 m) were arranged between Φ1250 grouting retaining piles to form a continuous waterproof curtain. The soil-mixed piles with a cement content of 15 % not only blocked the horizontal seepage of perched groundwater but also enhanced the lateral stiffness of the soil around the piles, consistent with the elastic foundation assumption in the theoretical model in Section 2.1 [10].

3.2. Engineering and hydrogeologic

According to the drilling data, the stratum of the proposed site area consists of

- Quaternary Holocene Artificial Fill (Q4ml)
- Quaternary Holocene Floodplain (Q4al+pl)
- Quaternary Upper Pleistocene Floodplain (Q3al+pl)
- Quaternary Upper Pleistocene Residual Layer (Q3el).

The predominant lithology includes heterogeneous fill, silty clay, clay, and red clay. The values of physical parameters of each layer

are shown in Table 1. The values of physical parameters of each soil layer were selected based on the *Geotechnical Engineering Survey Report for Construction Drawing Design of Wuhan Optics Valley Centre City Natural Gas Distributed Energy Project*, and the values of some parameters are shown in Table 1. The excavation base lies on a clay layer, and the characteristic value of the ground-bearing capacity meets the design requirements, allowing it to serve as the natural foundation for the excavation. Within the depth range revealed by the site"s exploration boreholes, the groundwater was identified as perched groundwater. This perched groundwater was predominantly distributed within the low-lying filled regions in the southwestern portion of the site, and the primary recharge mechanism was vertical infiltration of atmospheric precipitation. The site lacked a unified free-water surface.

Because of its limited volumetric extent and restricted spatial distribution, confined to mainly localised areas in the southwestern part of the site, coupled with minimal seasonal fluctuations in the water level caused by precipitation, perched groundwater exerts only a negligible influence on excavation construction. This negligible impact can be reasonably disregarded in the design and construction analysis of a project, because it is constrained in scope, insignificant in magnitude, and readily manageable through conventional dewatering measures, posing no substantive threat to the stability or safety of the excavation.

Table 1. Values of parameters for each soil layer in numerical simulation

Material	H [m]	γ_{unsat} [kN·m^{-3}]	E′ [MPa]	C′ [kPa]	φ [°]
Filling	4.8	19.0	8.9	36	13.4
Silty clay	5.0	19.3	8.4	40	13.5
Clay	4.0	19.3	12.1	54	14.7
Red clay	11.2	18.3	19.9	84	16.4

Note: All soil parameters listed in Table 1 were selected for drained conditions, consistent with the long-term construction process of the project (excavation duration > six months) and stratum permeability characteristics.

Clayey soil layers (silty clay, clay, and red clay)

For this solis with high cohesion (c = 40–84 kPa), the presence of an internal friction angle (φ = 13.5°–16.4°) is in line with the geotechnical test results of undisturbed soil samples. In reality, clayey soils are not purely cohesive (undrained φ = 0) but exhibit weak frictional characteristics owing to particle arrangement and minor sand content [10]. This is particularly true for the red clay used in this project (derived from the residual weathering of granite), which contains fine sand particles that impart a nonzero internal friction angle [13].

The drained condition assumption

This assumption is applicable here because the project adopts step-by-step excavation with temporary drainage measures (e.g., dewatering wells in the excavation), which allows sufficient time for pore water pressure dissipation in clayey soils, consistent with the drained analysis framework of the hardening soil model (HS model) used in the finite element simulation [8].

3.3. Intrinsic modelling and parameters

The finite element simulation was performed using Plaxis 3D, and a HS model was adopted to represent all strata in the numerical model [10]. Owing to the structural characteristics and anisotropy of the soil, its actual elastic modulus is greater than the compression modulus. Based on engineering experience, the actual elastic modulus of the soil in the excavation can be assumed to be two to five times the compression modulus of the soil.

Table 2. Parameter values for the HS model

	①	②	③	④
Materials	Fillings	Silty clay	Clay	Red clay
Thickness [m]	4.8	5.0	4.0	11.2
γ_{unsat} [kN·m^{-3}]	19.0	19.3	19.3	18.3
Kohezija (C) [kPa]	36	40	54	84
The angle of internal friction (φ) [°]	13.4	13.5	14.7	16.4
E_s^{1-2} [kPa]	8.9	8.4	12.1	19.9
ψ	0	0	0	0
E_{oed}^{ref} [kPa]	8.9	8.4	12.1	19.9
E_{50}^{ref} [kPa]	8.9	8.4	12.1	19.9
E_{ur}^{ref} [kPa]	35.6	33.6	48.4	79.6
m	0.8	0.8	0.8	0.8
R_f	0.9	0.9	0.9	0.9
R_{inter}	0.65	0.65	0.65	0.65
ν	0.2	0.2	0.2	0.2
Drainage state	drainage	drainage	drainage	drainage

The compression modulus of the soil, cohesion, angle of internal friction, and other parameters were obtained from the geotechnical test report table in the *Geotechnical Engineering Survey Report on Construction Drawing Design of Wuhan Optics Valley Centre City Natural Gas Distributed Energy Project*, and the tensile strength of the soil was taken as zero.

The HS model is adopted as the intrinsic model of the soil body, and the soil parameters were determined according to the parameters given in Table 1. The soil shear expansion angle ψ was set to 0 because the internal friction angle φ of each layer of the soil body was less than 30° [14]. The unloading Poisson"s ratio of the soil ν was set as 0.2. The stiffness parameter of the soil was determined as follows: The reference tangent compression modulus E_{oed}^{ref} was determined according to the compression modulus (E_s^{1-2}) range of 100–200 kPa given in the project investigation report [15], i.e., $E_{oed}^{ref} \approx E_s^{1-2}$. The reference tangent modulus E_{50}^{ref} was taken equal to the reference tangent compression modulus E_{oed}^{ref} [16], and the unloading reloading modulus E_{ur}^{ref} was set as four times the reference tangent modulus E_{50}^{ref} [17]. The power index *m* for each stiffness parameter is listed in Table 2 (0.8 for cohesive soils and 0.5 for sandy soils) [14]. All damage ratios (R_f) were set as 0.9.

Since both the retaining piles and basement wall were simulated by solid units, the solid units were given the concrete material parameters. In the actual project, when the retaining piles are driven into the ground, the cement slurry should be injected between the piles to reduce excavation deformation of the during excavating and prevent soil leakage between the piles. In Plaxis 3D, a linear elastic model is generally used to represent both concrete and cement slurry. Therefore, the parameters of the concrete and cement slurry in this numerical simulation model are determined according to Table 3. Because this study primarily focused on the stress behaviour of the retaining piles, the elastic modulus of the cement slurry was set significantly lower than that of concrete to avoid overestimating stiffness, which could otherwise distort the simulated deformation and force response of the retaining piles

Table 3. Parameter values for each soil layer in numerical simulation

Materials	Drainage type	γ_{unsat} [kN/m³]	Elastic modulus (*E*) [kPa]	ν
Concrete	non-porous	25	$31 \cdot 10^6$	0.1
liquid cement	non-porous	12	$4 \cdot 10^3$	0.1

3.4. Model building

To verify the reasonableness of the analytical solution for the "pile-wall" structure, a finite element model was established for this project, based on both the project data and the numerical simulation of an excavation project in a previous study [18]. The model included the basement wall, perimeter piles, foundation base plate, foundation roof plate, and connection node between the top and bottom, and the specific model is shown in Fig. 7.

The specific excavation model dimensions are shown in Fig. 8; Fig. 8a shows the front view of the model, while Fig. 8b shows the top view.

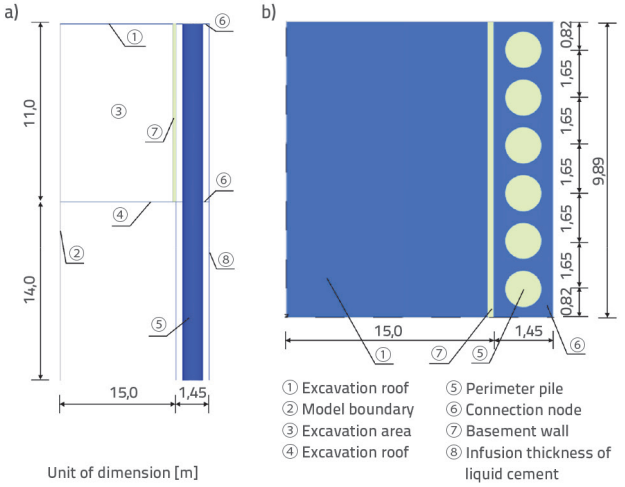

Figure 7. Dimensions of the finite element model

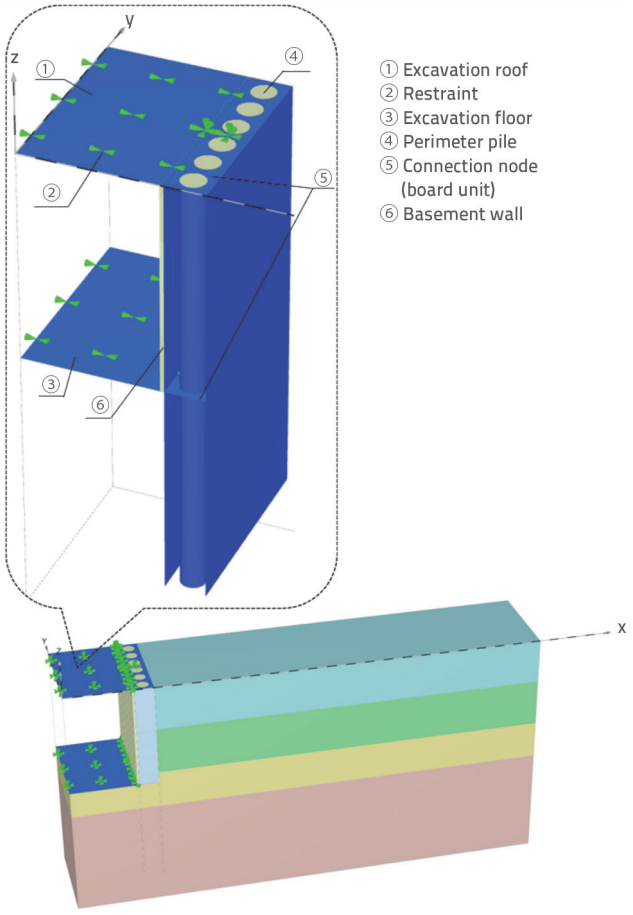

Figure 8. Integral finite element model of the "pile-wall" structural system

Among them, the basement wall and retaining row piles are simulated by solid units, and the excavation floor, excavation roof, and the connection nodes are simulated by slab units. The simulation of each component of the finite element model is shown in Table 4.

Table 4. Parameter information of the model components

Member	Analog unit	γ_{unsat}	H	E
Excavation roof	Plate unit	25	0.4	4E8
Excavation floor	Plate unit	25	0.4	4E8
Connection node	Plate unit	25	0.2	2.1E8

Because the connection node simulated by a point-to-point anchor unit in Plaxis 3D can only view the axial force, the bending moment and shear force of the connection node cannot be viewed Because this study primarily focused on the stress behaviour of the retaining piles, the elastic modulus of the cement slurry was set significantly lower than that of concrete to avoid overestimating stiffness, which could otherwise distort the simulated deformation and force response of the retaining piles. This can be reflected through the plate unit of the internal force of the bending moment and shear force of the connection node. For the excavation bottom and top plates, the stiffness is significantly large in the actual project; hence, the deformation along the X-direction can be almost ignored. Consequently, these plates can be regarded as a hinged support [19]. Therefore, in the model, X-direction fixed constraints are applied to the excavation top and bottom plates, to prevent displacement in the X-direction caused by the pit bottom and top plates. Thus, the hinged support is effectively simulated.
The model generated 56,932 cells and 130,127 nodes in the meshing stage. During excavation, the water head decreased to 2 m below the excavation surface; in other words, the effect of the ground water in the model was not considered. The step-by-step construction simulation of the finite element model was divided into five stages: installation of the retaining piles into the soil, excavation of the pit, construction of the excavation floor, construction of the basement wall and connection nodes, and construction of the excavation roof. The structural elements corresponding to each stage were activated sequentially in accordance with the construction process. Thus the "pile-wall" structural system was simulated, and the result of the finite element numerical calculation is given below together with the derivation of the formulae.

4. Comparison of finite element and analytical solutions

4.1. Retaining pile comparison

Figure 9 presents a comparison between the analytically derived bending moment equations and the finite element simulation results for the retaining piles when connection nodes (pins) are present at the top and bottom of the pile–wall structure.
Figure 10 illustrates a similar comparison for the case without connection nodes, highlighting the differences between the theoretical derivation and numerical simulation results.

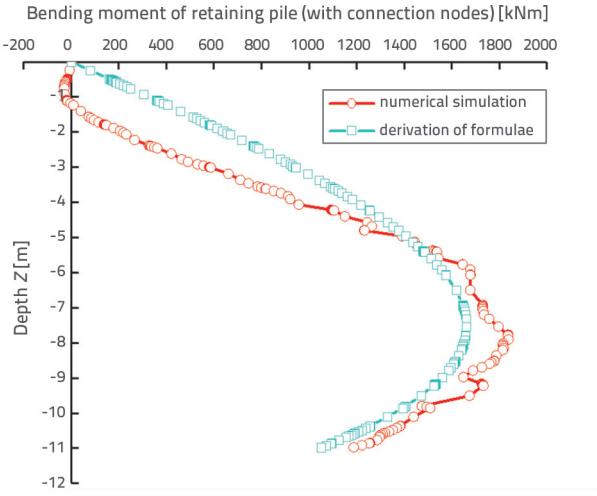

Figure 9. Bending moment diagram of perimeter piles with connection nodes

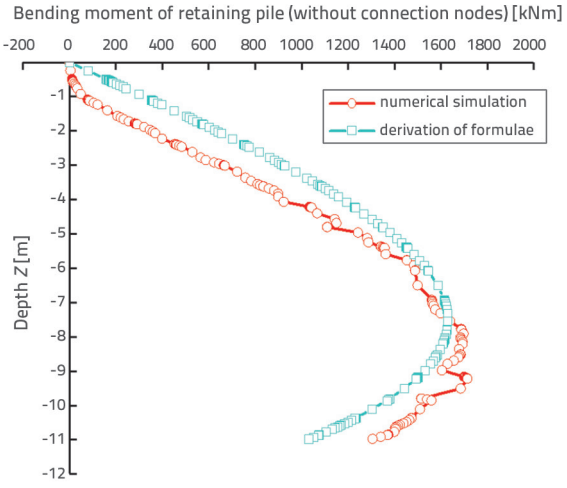

Figure 10. Bending moment diagram of perimeter piles without connection nodes

Based on the curve fitting results of the perimeter piles with and without connection nodes (pins), the finite element simulation and formulae are in good agreement. The maximum bending moment of the perimeter piles with connection nodes was approximately 1884 kNm in the finite element simulation and approximately 1693 kNm in the analytical model, both showing a better fit to the bending moment peak. For the perimeter piles without connection nodes, the corresponding maximum bending moments were approximately 1743 kNm (simulation) and 1665 kNm (formulae). These results indicate that the bending moment of the perimeter pile with connection nodes is larger than that without connection nodes, suggesting that the connection nodes can increase the maximum bending moment carried by the perimeter pile by about 141 kNm.

4.2. Basement wall comparison

Figure 11 presents a comparison between the analytical results derived from the formulae and the finite element simulation

results for the bending moments of the basement wall when connection nodes are present (pins) at the top and bottom of the "pile-wall" structure. Figure 12 illustrates a similar comparison for the bending moments of the basement wall without connection nodes.

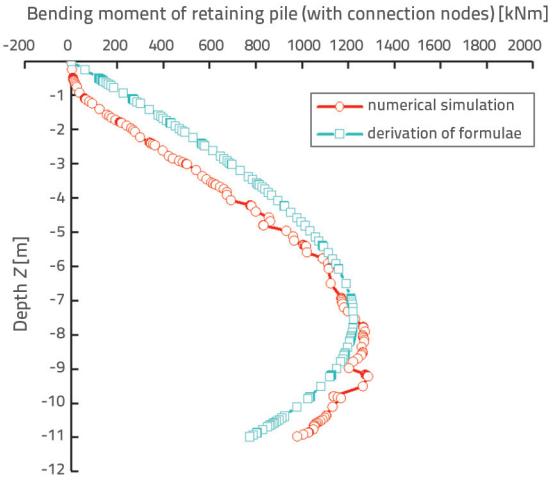

Figure 11. Bending moment diagram of the basement wall with connection nodes

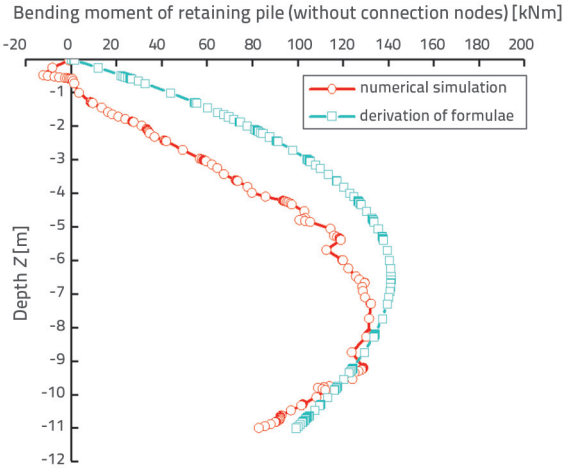

Figure 12. Bending moment diagram of the basement wall without connection nodes

Based on the curve fitting result of the basement wall with and without connection nodes (pins), the finite element simulation and formulae show good agreement. The maximum bending moment of the basement wall with connection nodes obtained from the finite element simulation is approximately 126 kNm, while the corresponding value obtained from the formulae is approximately 122 kNm, both showing a better fit at the bending moment peak. For the basement wall without connection nodes, the maximum bending moment obtained from the finite element simulation is approximately 137 kNm, and that from the formulae is approximately 141 kNm. A comparative analysis these results show that the bending moment of the basement wall with connection nodes is larger than that without connection nodes, suggesting that connection nodes can increase the bending moment carried by the basement wall by about 11 kNm.

4.3. Connection node comparison

Regarding the internal force of the connection node, the bending moment of the connection node derived from Eq. (24) can be obtained by substituting into the dimension parameters of the finite element model with the specific value of the connection node"s bending moment of 2239.6 kNm. In the finite element simulation, the internal force of the connection node was obtained by extracting the internal force of the plate element reflecting the internal force of the connection node. The bending moment of the connection node in the Y-direction (i.e., the direction of longitudinal extension of the connection node) is shown in Fig. 13. As shown in Fig. 13, the bending moment peak of the connection node in the finite element simulation is 2199.64 kNm. This value does not exceed the peak connection node moment derived analytically (2239.6 kNm). Thus, the equation used to derive the bending moment of the connection node is validated as feasible.

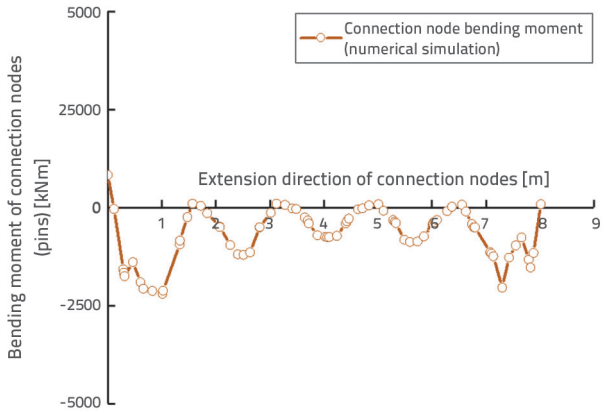

Figure 13. Finite element simulation of connection node in bending moment in direction of extension

In summary, comparison of the finite element simulation and formula derivation results indicate that:

- The analytical formulae for the retaining pile and basement wall closely match the numerical simulations in terms of the distribution pattern and peak value.
- When there are no connection nodes, the retaining pile and basement wall are not integrated, causing the external soil and water pressure to be transferred to the basement wall through the retaining pile. Hence, the basement wall is subjected to large soil and water pressure, which may lead to engineering hazards.
- With connection nodes, the retaining pile and basement wall act as an integrated system , allowing the retaining pile to retain more soil and share and resist a larger portion of the external soil and water pressure. Consequently, the bending moment of the retaining pile increases compared with that without the connection nodes, while the bending moment of the basement wall decreases.

- For the internal force generated by the connection nodes between the retaining pile and basement wall, the finite element simulation results closely match the peak values compared with the derivation results of the formulae with known parameters of the model. Thus, the theoretical formulae are confirmed to be reliable.

5. Conclusion

In this paper, a simplified model of the "pile-wall" structural system was developed through the combination of the retaining pile and basement wall. Furthermore, internal force equations of the pile-wall and its connection nodes were derived for cases with and without connection nodes. Subsequently, the internal force of the pile-wall structure system with and without connection nodes was analysed, and finite element numerical simulations were conducted using the Plaxis 3D software to verify and compare the theoretical formulae. The main conclusions are as follows:

- By modelling the retaining piles and basement wall as two EB beams with identical material properties but different cross-sectional dimensions, representing the connection nodes between the piles and wall as pins connecting the pile and wall, and treating the excavation roof and floor as hinged bearings restraining the displacement of the pile wall to the inner side of the excavation, the simplified calculation model of pile-wall structure effectively captures the actual engineering behaviour of the structure, as verified by the finite element numerical simulations. Using the material mechanics theory, the internal force formula of the pile wall and connection node were derived from equilibrium equations, physical equations, and geometrical relationships under the assumption of flat cross-sections. The good agreement between these formulae and the finite element simulation results which demonstrates their reliability and provides practical guidance for real-world projects.
- Comparison of the finite element simulation and formula derivation results shows a high degree of agreement in the distribution patterns of the retaining pile and basement wall. The curve trends of the numerical simulations and the derived formulas align closely. The error between the finite element simulation and formula derivation results is within 10.14 % for the retaining pile and within 3.18 % for the basement wall. The peak values of the internal forces of the connection nodes also closely match between the simulation and formula results, indicating that the derived internal force equations can reliably guide the design and analysis of specific pile-wall projects.
- In the numerical simulation of the excavation project, the maximum bending moment values of the perimeter pile with and without connecting nodes are about 1884 and 1743 kNm, respectively; furthermore, the maximum bending moment values of the basement wall with and without connecting nodes are about 126 and 137 kNm, respectively. Thus, the connecting nodes enable the perimeter piles to share an additional bending moment of about 141 kNm (bearing ratio: about 8.09 %), while the bending moment of the perimeter pile is reduced by about 11 kNm (bearing ratio: about 8.03 %). Therefore, the bending moment of the perimeter pile with connection nodes increases compared with that of the no-connection node case, whereas the bending moment of the basement wall with connection nodes decreases compared with that of the no-connection node case because the external soil and water pressure on the basement wall are largely transferred to the perimeter piles.

Acknowledgements

The authors thank the Shandong Electric Power Engineering Consulting Institute Corp. Ltd. for their financial support, and Professor Huanwei Wei et al. at Shandong Jianzhu University for their technical support.

REFERENCES

[1] Wu, Z.: Practice of dual purpose wall technique with auger drilling pressure-grouting pile in top-down method excavation, Chinese Journal of Underground Space and Engineering, 14 (2018) 1, pp. 308-314 + 356.

[2] Wang, W., Shen, J.: Design and analysis of unity of support piles and basement external walls, Chinese Journal of Geotechnical Engineering, 34 (2012) 1, pp. 303-308.

[3] Nie, G., Xu, M., Zhong, Z.: Elastic and elastoplastic bending of rectangular beams with variable stiffness along the axial direction, Scientia Sinica Physica, Mechanica & Astronomica, 41 (2011) 1, pp. 86-93, https://doi.org/10.1360/132010-802.

[4] Hu, Y., Wang, W., Shen, J.: Field monitoring and analysis of stresses for dual-purpose pile wall, Chinese Journal of Geotechnical Engineering, 37 (2015) 2, pp. 197-201.

[5] Wang, J., Li, D., Zhang, Z.: Practice of dual-purpose pile wall technique in deep foundation engineering, Journal of Anhui Jianzhu University, 29 (2021) 1, pp. 26-32.

[6] Zhong, C., Fu, J.: Design and analysis of structural key technology for the No. 8 block of Hongqiao Business District, Building Structure, 42 (2012) 5, pp. 106-109 + 61, https://doi.org/10.19701/j.jzjg.2012.05.022.

[7] Zhang, L., Li, H., Chen, Z.: Application of pile-wall composite structure in sandy soil foundation pits: A case study, Journal of Rock Mechanics and Geotechnical Engineering, 15 (2023) 2, pp. 412-421.

[8] Terzaghi, K., Peck, R.B.: Soil Mechanics in Engineering Practice, Second Edition, John Wiley & Sons, New York, 1967.

[9] Zheng, L., Sun, B., Li, P., et al.: The crack calculation and experiment of the clingy "pile-wall", Chinese Journal of Underground Space and Engineering, 14 (2018) 2, pp. 571-578 + 612.

[10] Liu, G., Wang, W.: Manual of Foundation Pit Engineering, Second Edition, China Construction Industry Press, Beijing, 2009.

[11] Cheng, C., Zhu , Y.: Theory of Elasticity, Shanghai University Press, Shanghai, 2005.

[12] Wu, X.: Analysis of bending deformations of bolted bimodulus-laminated beams, Journal of Central South University (Science and Technology), 46 (2005) 8, pp. 2871-2876.

[13] Chen, Y.M., Zhang, H.: Geotechnical properties of residual red clay in Wuhan area, Journal of Geotechnical Engineering, 41 (2019) 1, pp. 189-193.

[14] Wang, W., Wang, H., Xu, Z.: Experimental study of parameters of hardening soil model for numerical analysis of excavations of foundation pits, Rock and Soil Mechanics, 33 (2012) 8, pp. 2283-2290, https://doi.org/10.16285/j.rsm.2012.08.006.

[15] Zheng; X., Zhu, S.: Study on the wallboard diaphragm wall for foundation pit support, Journal of Lanzhou University of Technology, 49 (2023) 4, pp. 137-145.

[16] Wang, H., Song, E., Xu, M.: Hardening-soil model for underground construction, J T singhua Univ (Sci & Tech), 50 (2010) 3, pp. 351-354, https://doi.org/10.16511/j.cnki.qhdxxb.2010.03.017.

[17] Xie, J., Zeng, X., Hu, J.: Application of hardening soil model in deep excavations supported by pile anchor and pile braced composite supporting structures, Chinese Journal of Geotechnical Engineering, 36 (2014) 2, pp. 56-63.

[18] Liu, X., Wang, J., Zhou, X., et al.: Response of long-short supporting piles due to deep excavation in soil-rock combined strata, International Journal of Geomechanics, 24 (2024) 2, pp. 04023276, https://doi.org/10.1061/IJGNAI.GMENG-8587.

[19] Wu, C., Yu, J., Cao, X., Shen, W.: Study on design method of pile wall combination structure in a deep foundation pit considering deformation induced by excavation, Frontiers in Earth Science, 10 (2022), Paper 837950, https://doi.org/10.3389/feart.2022.837950.